

Article

Influence of Al Addition on the Microstructure and Wear Behavior of Laser Cladding FeCoCrNiAl_x High-Entropy Alloy Coatings

Yang Liu ^{1,2}, Zhixiang Xu ², Gaojie Xu ^{1,*} and Hongyong Chen ³

¹ Ningbo Institute of Materials of Technology and Engineering, Chinese Academy of Sciences, Ningbo 315201, China

² Faculty of Mechanical Engineering & Mechanics, Ningbo University, Ningbo 315211, China

³ Ningbo Institute of Zhongwu Laser and Photoelectric Technology, Ningbo 315000, China

* Correspondence: xugj@nimte.ac.cn

Abstract: In order to improve the wear properties of FeCoCrNi high entropy alloy (HEA), laser cladding was applied to fabricate FeCoCrNiAl_x HEA coatings with different Al additions. The Al-modified coatings exhibited excellent metallurgical bonding interfaces with the substrates. The microstructure of FeCoCrNiAl_{0.5} coating was the same as of the FeCoCrNi coating: face-centered cubic (FCC). However, the microstructure of FeCoCrNiAl was different: body-centered cubic (BCC) with more Al atoms distributed inside the grains. As the Al content in the coating was increased, the hardness increased as well from 202 to 546 HV_{0.2}, while CoF and wear rate decreased from 0.62 to 0.1 and from 8.55×10^{-7} to 8.24×10^{-9} mm³/(Nm), respectively. The wear mechanisms changed from the mixture of abrasive, adhesive, and oxidative wear patterns to the mixture of abrasive and oxidative patterns. Such a change indicates that the Al addition indeed improved the wear resistance of FeCoCrNiAl_x HEA coatings. Our results expand knowledge on HEA coating applications as wear-resistant materials in various applied industrial fields.

Keywords: laser cladding; FeCoCrNiAl_x; high entropy alloy coating; wear properties



Citation: Liu, Y.; Xu, Z.; Xu, G.; Chen, H. Influence of Al Addition on the Microstructure and Wear Behavior of Laser Cladding FeCoCrNiAl_x High-Entropy Alloy Coatings. *Coatings* **2023**, *13*, 426. <https://doi.org/10.3390/coatings13020426>

Academic Editors: Rafael Comesaña and Angela De Bonis

Received: 16 November 2022

Revised: 20 January 2023

Accepted: 9 February 2023

Published: 13 February 2023



Copyright: © 2023 by the authors. Licensee MDPI, Basel, Switzerland. This article is an open access article distributed under the terms and conditions of the Creative Commons Attribution (CC BY) license (<https://creativecommons.org/licenses/by/4.0/>).

1. Introduction

In 2004, J.W. Yeh et al. [1] and Cantor et al. [2] described a concept of high-entropy alloys (HEAs), which contain five or more principal elements with contents in the 5–35 at% range. Other trace elements could be present as well but at levels below 5 at%. The unique properties of HEAs (such as high entropy, lattice distortion, hysteretic diffusion, and “cocktail” effects) make them superior (in terms of strength, toughness, wear, and corrosion resistances) to traditional alloys [3–5].

Studies of Al-containing HEAs revealed that Al levels significantly affect the microstructure and mechanical properties of the resulting material [6]. In some cases, Al's addition to Fe-based HEAs promoted the formation of the body-centered cubic (BCC) phase [7–10]. Sharma et al. [7,8] analysis of Al_xFeCoCrNi HEAs revealed that Al addition activated the diffusive transformations from molten to crystalline phases (at lower Al addition levels) or from molten to amorphous transitions (at higher Al contents). Ogura et al. [9] demonstrated (using first principles electronic structure calculations) that an increase in the Al contents in HEA alloys reduces the energy difference between the FCC and BCC phases. Feng et al. [10] experimentally demonstrated that when Al was added (up to 5%) to FeCoCrNi, a material with improved plastic deformation was obtained.

Coatings fabricated by laser metal deposition (also known as laser cladding) exhibit high density and good metallurgical bonding with the matrix, which made laser cladding a very popular method in industrial applications [11–13]. The wear properties of HEA coatings prepared by laser cladding could be further improved by adding ceramic particles

(e.g., TiC [14], NbC [15], WC [16]), which act as reinforcing ex-situ phases. The addition of these trace phases also changes other HEA properties such as phase transition, grain refinement, etc. For example, Cai et al. [14] analyzed FeCrNiCoMn+xTiC HEA coatings prepared by laser cladding and discovered that TiC particles promote the formation of low-angle grain boundaries while inhibiting the high-angle grain boundaries. The increase in TiC content reduces the grain size and increases the dislocation density, while their pinning effect improves the overall coating strength. Li et al. [15] fabricated AlCoCrFeNi+xNbC HEA coating by laser cladding. The addition of the NbC particles forced the FCC \rightarrow BCC transition. Additionally, the presence of the NbC particles at the grain boundaries provided a strong pinning effect, which also contributed to the grain growth inhibition, hindered dislocation slip, and plastic deformation, which all, in turn, significantly improved the hardness and wear resistance of the AlCoCrFeNi coating.

Laser metal deposition offers great flexibility in coating fabrication, which makes it very easy to manufacture coatings with various compositions and contents. In fact, this was achieved with great success for the HEA-based coatings, which demonstrated excellent performance and unique properties [17–20]. The popularity of laser cladding in the manufacturing of advanced coatings gained a lot of interest from the scientific and engineering communities. Thus, a lot of data is accumulated on different aspects related to coatings' properties obtained by laser metal deposition. For example, grain refinement and phase transformations of high-entropy CoCrFeNi-HEA-based coatings typically occur when after adding Al, Mo, Nb, Cu, B, or Si. As a result, the strength and hardness as well as deformation and wear resistances of the modified CoCrFeNi coatings are better than those of their original counterparts. Specifically, FCC-structured CoCrFeNiSi_x HEA coatings became BCC-based when Si was added [17]. Increased Al content in the single-FCC phase FeCoCrNiCuAl_x HEA coating caused it to become single-BCC phase material [18]. Liu et al. [19,20] reported that adding traces of W and Nb into FeCoCrNi enhances its wear resistance at high temperatures.

Various post-heat treatment methods are used to improve FeCoCrNi HEA properties [21]. However, such methods might become expensive if used on a large scale. Thus, the alloying element addition to tune the microstructure and wear/corrosion resistances of FeCoCrNi HEA coatings without the need for involved post-treatment techniques would be an efficient low-cost alternative [22,23]. Therefore, our work focuses on the analysis of the properties (microstructure and wear resistance) of FeCoCrNiAl_x ($x = 0, 0.5, 1$) HEA coating obtained by laser cladding. Our results point to a feasible way to improve and tune the wear properties of the laser cladding HEA coatings by regulating the contents of elements. With such improved properties, HEA coatings can expand their industrial applications as anti-abrasion materials on products such as bearings, gears, screws, etc.

2. Experimental Details

2.1. Materials and Laser-Cladding Equipment

Pieces of 45# steel ($\varnothing 50$ mm \times 10 mm) acted as substrates. Each plate was polished with 200–3000 grit SiC papers in sequence, followed by ultrasonic cleaning in anhydrous ethanol. The raw materials were FeCoCrNiAl_x ($x = 0, 0.5, 1$) HEA powders with 200 mesh average particle sizes. Al content was confirmed experimentally (see Figure 1a,b). The coatings were deposited using a coaxial powder-feeding laser cladding device, equipped with a 4 KW continuous fiber laser with ≤ 2 mm spot diameter. The laser cladding process and FeCoCrNiAl HEA coating are schematically shown in Figure 1c,d, respectively. The tracks for the single-pass experiments were fabricated to be 30 mm long. They were then cut into several sections for further analyses. The samples prepared during the coating experiments were 30 mm long and ~ 12 mm wide (achieved in 12 passes with the 1200 W laser power, 8 mm/s scanning speed, 40% overlap ratio, and -10 mm off-focus distance). All details and parameters of the laser cladding are summarized in Table 1.

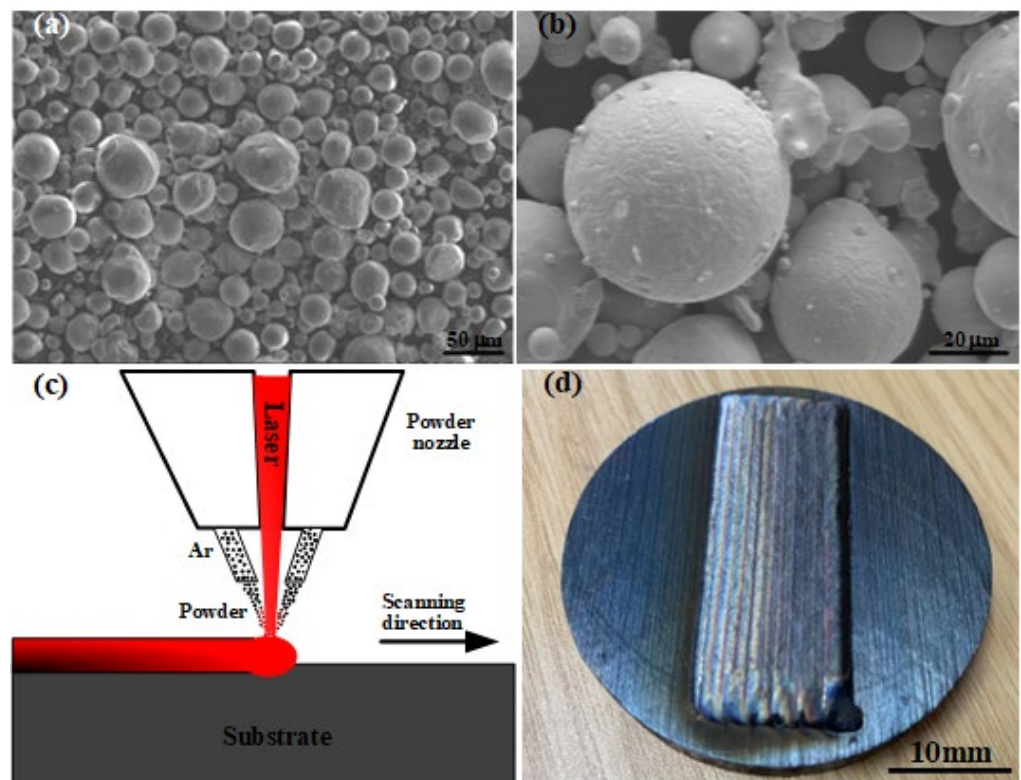


Figure 1. (a,b) Morphology of FeCoCrNiAl HEA powder, (c) schematic diagram of laser cladding process, (d) FeCoCrNiAl HEA coating.

Table 1. Laser cladding process parameters for FeCoCrNiAl HEA coatings.

Laser Power/W	Scanning Speed/(mm/s)	Overlap Ratio/%	Off-Focus/mm	Powder Feeding Speed/(g/s)	Protected Air Flow/(L/min)
1200	8	40	−10	7	15

2.2. Sample Characterization

The samples were cut perpendicular to the scanning direction, after which the cut surfaces were ground with 100–2500 grit SiC papers sequentially followed by polishing with 1 μm diamond paper and etching in HCl:HNO₃ mixture (3:1) for ~30 s. The formed phases were characterized by X-ray diffraction (XRD) performed using Bruker D8-ADVANCE instrument equipped with Cu-K α radiation and operated at 40 kV and 40 mA. The spectra were recorded at 0.02° step size and 2°/min scanning speed. The microhardness was measured using a Vickers hardness tester (WILSON VH1102, Lake Bluff, IL, USA). The data were collected at 100 μm intervals starting from the surface down to the substrate at 200 g load and 15 s applied load time. Data for each point was collected three times. The average was reported as a final value. Wear tests were performed on an Pin-disk friction wear tester (SFT-2M, Changzhou, China) using a 5 mm diameter GCr15 steel ball at 10 N load, 400 r/min rotation speed, and 30 min testing time. Before wearing, the coatings were milled with a flat grinding machine and then ground with SiC papers with 1000 grit. The microstructures of pristine and worn surfaces were analyzed using a confocal laser scanning microscope (Lecia TCS SP2/AOBS, Solms, Germany) and scanning electron microscope (Hitachi SU5000, Tokyo, Japan).

3. Results and Discussions

3.1. Macro/Micro Characteristics of the Cladding Tracks

The surfaces of the cladding tracks of the FeCoCrNiAl_x ($x = 0, 0.5, \text{ and } 1$) were smooth with minimum unmelted powder particles (see Figure 2). No spatter generated during cladding was observed as well. The dimensions of cladding tracks (with the width L and height h_1), molten pool depth h_2 , and dilution rate $\eta = \frac{h_2}{h_1+h_2}$ are summarized in Table 2. With the increase of Al content, the height and width of the cladding track gradually decreased because Al reflects the laser beam, which reduces the energy absorbed by the melt pool. This, in turn, leads to pore and crack formation in the coatings [24], in which the powder particles might remain if not removed by the protective gas flow. Additionally, the dilution rate of the cladding tracks increased aggravates this tendency very likely because of the lower (relative to other elements in the coating) melting and vaporizing points of Al. During the cladding process, Al atoms evaporate easier under the laser beam, which forces the liquid-phase flow in the molten pool as well as its stirring by the high-pressure steam. These factors enhance the Marangoni convection in the molten pool, which leads to a decreased height of the cladding track, and an increased dilution rate [6,9].

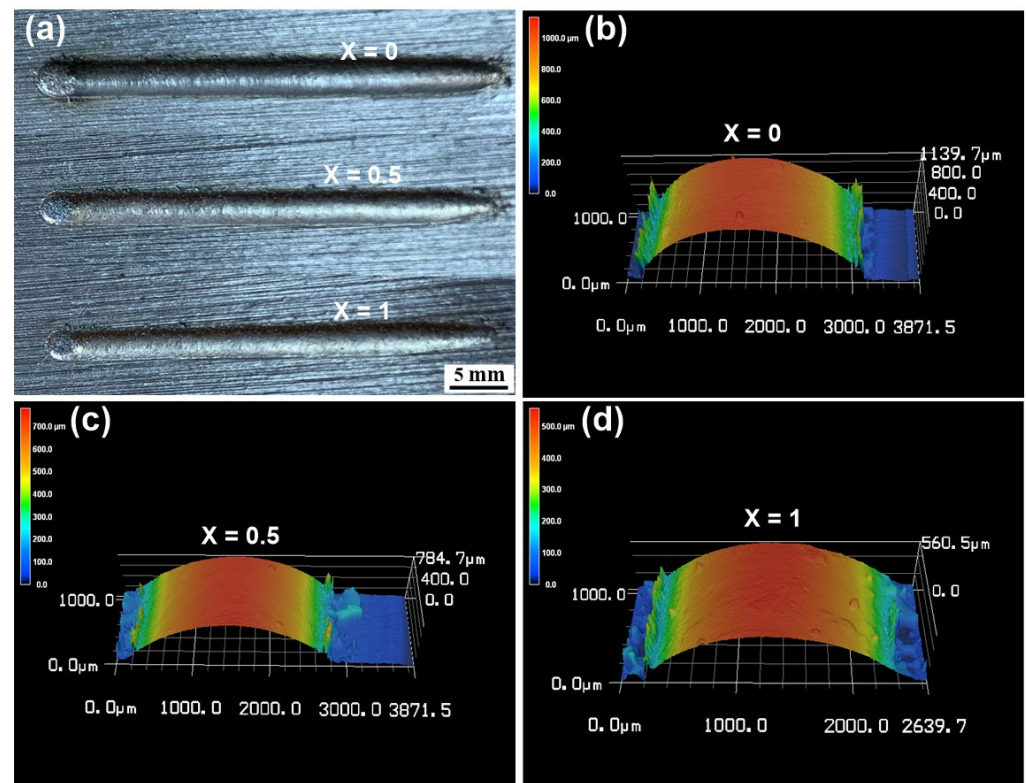


Figure 2. 3D morphologies of FeCoCrNiAl_x single cladding tracks with different Al contents. (a) morphologies of tracks, (b–d) the reconstructed 3D morphologies of tracks with different Al contents.

Table 2. Geometry dimension sizes and dilution rate of FeCoCrNiAl_x single cladding tracks.

Items	$x = 0$	$x = 0.5$	$x = 1$
$L/\mu\text{m}$	2830	2540	2210
$h_1/\mu\text{m}$	1139.7	784.7	560.5
$h_2/\mu\text{m}$	332	314	290
$\eta/\%$	22.5	28.6	33.1

Cross-line EDS of the FeCoCrNiAl coating cross-section starting from the surface to the substrate showed no cracks or holes (see the SEM image in Figure 3a), which indicates

excellent metallurgical bonding of the coating to the substrate. Fe, Co, Ni, Cr, and Al elements were distributed homogeneously within the coatings (see Figure 3b), which confirms very minimum atom segregation or aggregation. The Fe content in the coating zone was the highest out of all other elements because Fe in the substrate was melted during laser cladding and became incorporated into the coating. Fe content in the bonding zone increased almost linearly, while the content of other elements decreased, which indicates sufficient diffusion of the elements between the coating and substrate and ensures excellent metallurgical bonding between the coating and substrate.

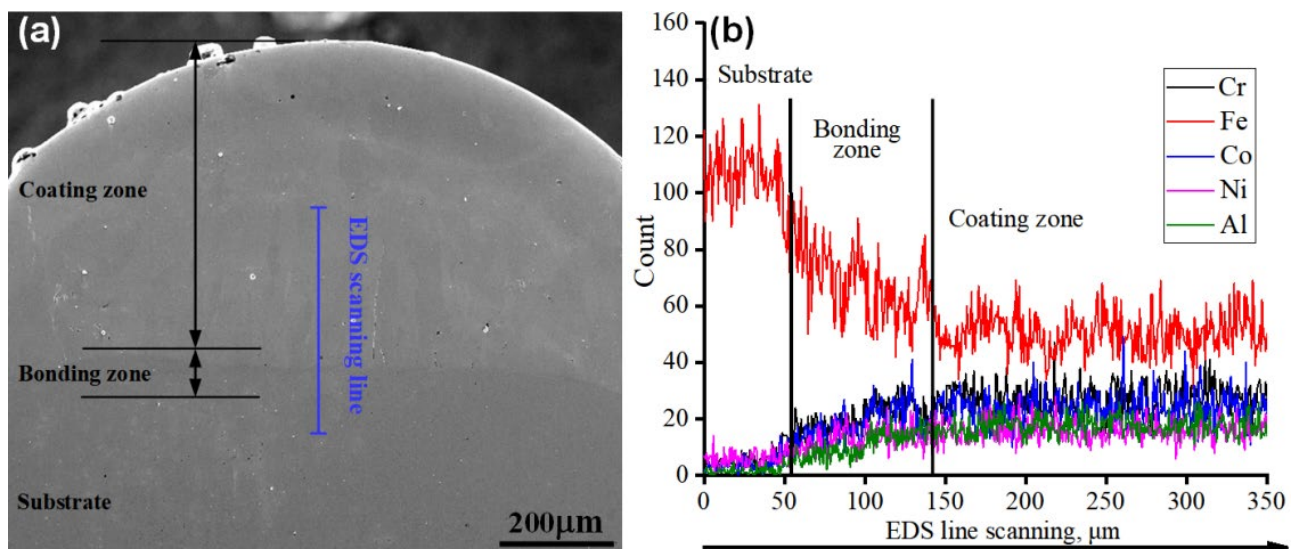


Figure 3. (a) SEM morphology of cross-section of the FeCoCrNiAl single cladding track, and (b) element distribution along the height direction.

3.2. Phase and Microstructure of the FeCoCrNiAl_x Coatings

XRD of the FeCoCrNiAl_x HEA coatings revealed that FeCoCrNi and FeCoCrNiAl_{0.5} coatings only contain FCC phase (see Figure 4) judging by prevailing (111), (200), (220), (311), and (222) diffraction peaks. At the same time, the FeCoCrNiAl phase contained only BCC solid solution phase, which contains diffraction peaks (110), (200), (211), and (220). Al atoms dissolve in the matrix, forming solid solutions and expanding the lattice. At small contents, these changes are not affecting the underlying matrix structure [25]. However, at certain threshold contents, Al presence in the host matrix causes enough lattice distortion to cause FCC → BCC phase transition. By comparing the PDF cards, it can be found that the BCC phase has the substitutional solid solution as AlNi, whereas the FCC phase has Al as an interstitial solid solution. The phase transformations of solid solutions in the FeCoCrNiAl_x HEA occur due to the high entropy nature of the alloy. Compatibility between components with high mixing entropy increases, which, in turn, prevents the formation of intermetallic compounds in the HEAs. Thus, the formation of simple solid solutions is more energetically favorable [26,27].

The microstructure of the FeCoCrNi coating was mainly composed of columnar grains (see Figure 5a,b). The microstructure of the FeCoCrNiAl_{0.5} contained columnar and cellular grains with obvious boundaries. These differences were attributed to the direction of the heat losses dominating during the coating deposition. The direction of the grain growth during solidification is typically opposite to the heat flow current. Thus, solute atoms will gather in front of the solid-liquid interface, which will change the solidification equilibrium temperature. When the actual temperature at the front edge of the solid-liquid interface is lower than the equilibrium temperature, component supercooling occurs at the solid-liquid interface, and cellular grains form. The laser cladding possesses a significantly higher solidification rate than the casting process. Thus, quasi-directional solidification conditions

at the solid-liquid interface occur easier, which is conducive to the formation of columnar grains perpendicular to the quasi-directional solidification direction [28,29].

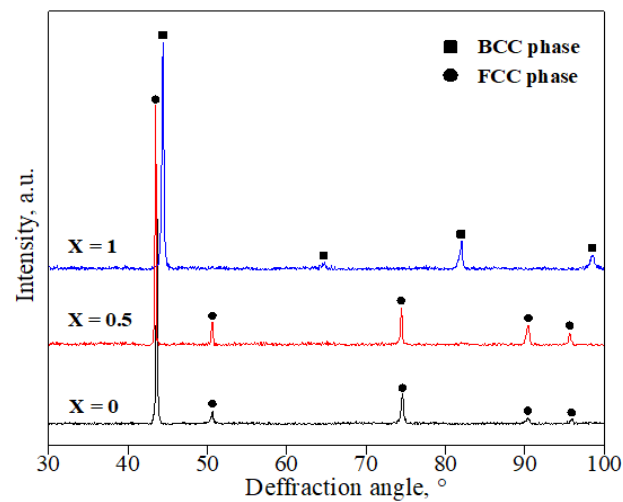


Figure 4. XRD patterns of the coatings with different Al contents.

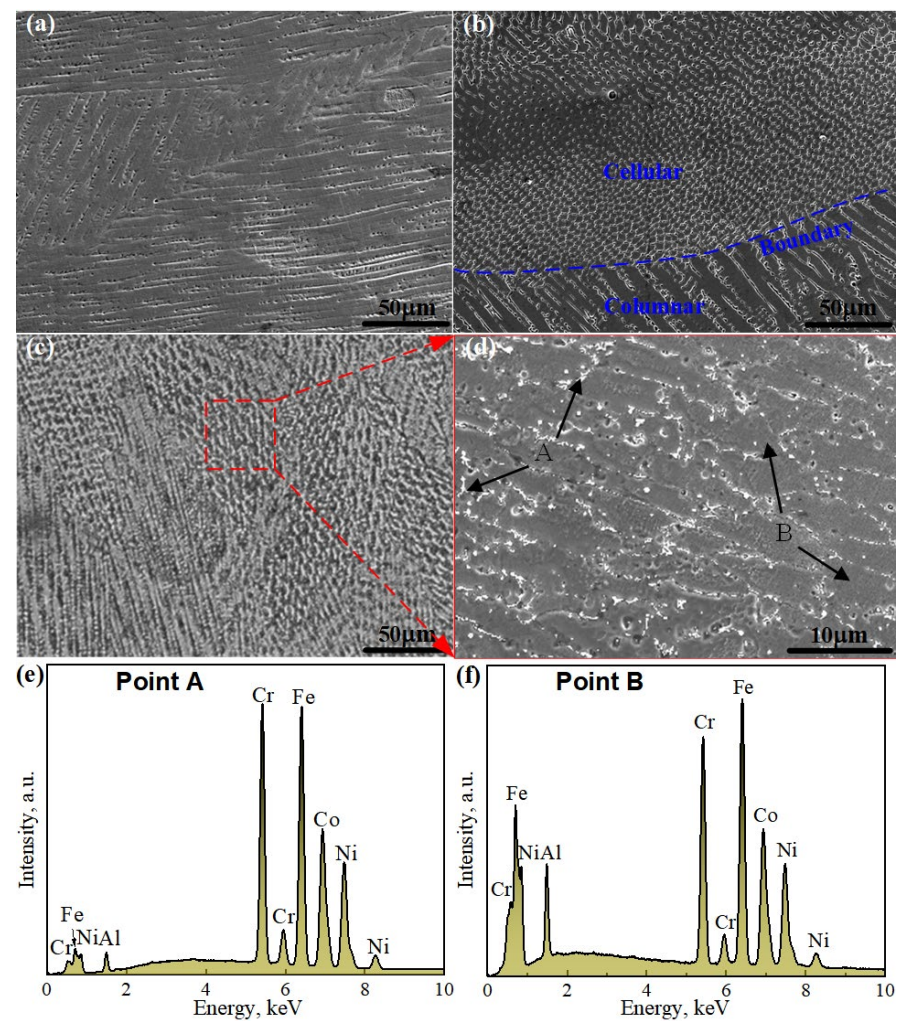


Figure 5. SEM images of cross-sections of single cladding tracks of (a) FeCoCrNi, (b) FeCoCrNiAl_{0.5}, (c,d) FeCoCrNiAl, (e,f) EDS of points A and B indicated in (d).

The microstructure of FeCoCrNiAl coating mainly consisted of equiaxed grains according to the SEM, shown in Figure 5c,d. Corrosion pits were also observed on the surface of the coating because we used very aggressive corrosion media to remove the cladding layer of the HEAs. EDS point analysis at grain boundaries (point A) and interiors (point B) showed lower Al contents at the grain boundaries than in the grain interiors (see Figure 5e,f). Thus, Al mainly accumulated in the grain interiors, which agrees with the literature data [30,31]. This phenomenon could be explained by the lattice distortion during the HEA solidification that occurred due to the presence of large Al atoms. As a result, atomic diffusion in the molten pool was inhibited. This is also known as a HEA hysteresis diffusion effect [32]. Combining these observations with the XRD results, we conclude that the BCC-structured FeCoCrNiAl coating formed as a result of Al-containing metal compounds inside the grains.

3.3. Microhardness of FeCoCrNiAl_x HEA Coatings

The average microhardness of the FeCoCrNi coatings was only 202HV_{0.2} (see Figure 6), which is even lower than that of the underlying substrate (210HV_{0.2}). As the Al content in the coating increased to 1, the microhardness increased substantially to 546 HV_{0.2}. Thus, by adding Al, we significantly improved the mechanical properties of this HEA. This phenomenon could be explained by the large size of Al atoms: when they occupy the lattice dot positions, the crystal lattice becomes distorted, which makes it more difficult for the material to deform. As a result, a stronger solid-solution-based matrix becomes harder [9]. Additionally, our microscopical analysis of the FeCoCrNiAl coatings revealed many fine equiaxed 5–10 μm grains (see Figure 5c,d), which is also a contributing factor to the enhanced hardness. Thus, the incorporation of Al into the FeCoCrNi matrix improves its hardness by (1) inducing FCC → BCC phase transition, (2) distorting the lattices, and (3) fine-grained strengthening.

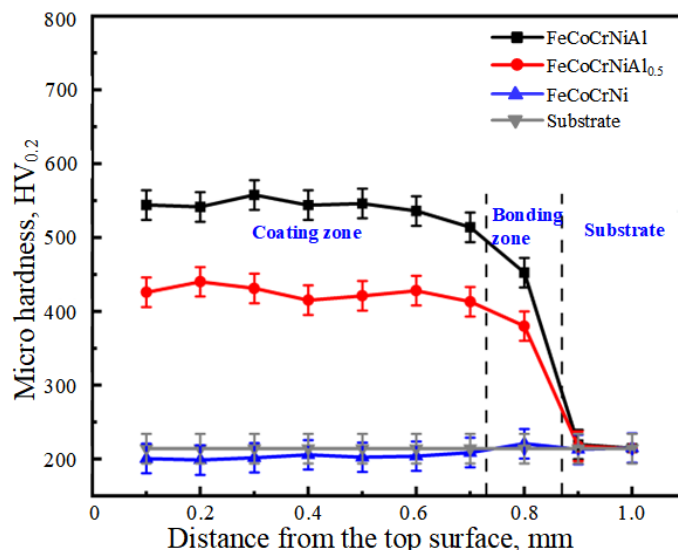


Figure 6. Micro hardness of single cladding tracks from coating top surface to substrate, the distance between the measuring points is about 100 mm.

We distinguished three zones with varying hardness (from the top surface of the coating to the substrate): coating zone, bonding zone, and substrate. The hardness in the coating zone is relatively stable throughout the whole sample size. The hardness in the bonding zone decreases substantially due to the dilution of the initially hard coating by the substrate atoms. Additionally, we observed that the hardness in the bonding zone of the FeCoCrNiAl coating decreased more than in the bonding zone of the FeCoCrNiAl_{0.5} coating (with less Al). This phenomenon can be explained by the induced (by Al presence)

Marangoni convection in the molten pool, which, in turn, facilitates the atom exchange at the interface.

3.4. Wear Properties of FeCoCrNiAl_x HEA Coatings

The coefficient of friction (COF) curve of FeCoCrNi HEA coating exhibited periodic fluctuation (see Figure 7) very likely because due to the low hardness of this coating, large abrasive debris and adhesions were continuously generated and removed repeatedly during the wear process (as illustrated in the Figure 8a). This caused a varying contact between the grinding ball and the worn surface, which, in turn, translated into fluctuating COF curve. At the same time, the COF curves of the coatings containing Al were stable.

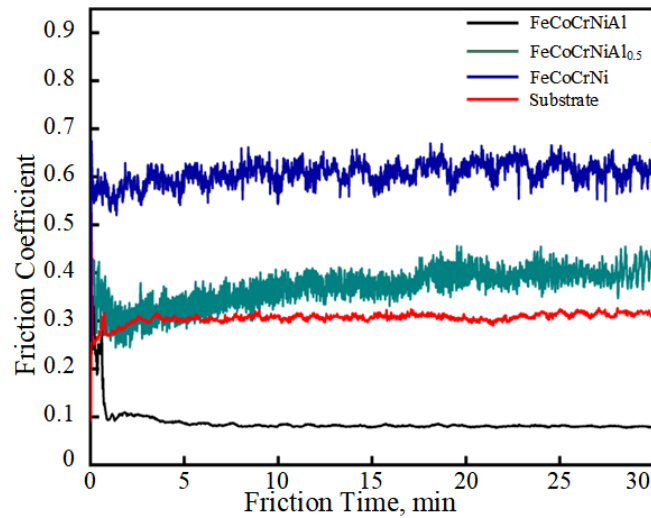


Figure 7. Coefficients of friction of the coatings with different Al contents.

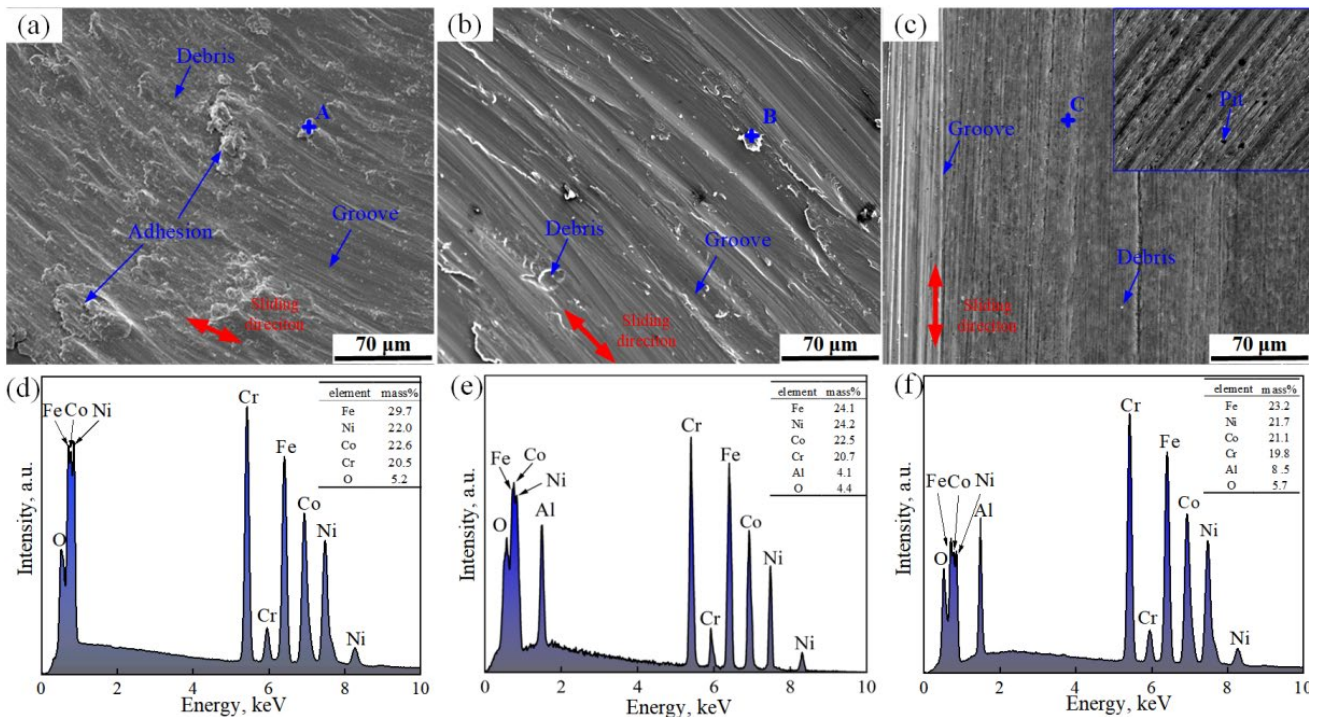


Figure 8. SEM images of worn surfaces and elements of the coatings of (a,d) FeCoCrNi, (b,e) FeCoCrNiAl_{0.5}, (c,f) FeCoCrNiAl.

Values of worn width, depth, and wear rate obtained during the COF tests for the FeCoCrNiAl coating were much lower than for the FeCoCrNi and FeCoCrNiAl_{0.5} coatings (see Table 3). This phenomenon could be explained by smaller grains and higher hardness of the FeCoCrNiAl coating. These properties ensure that FeCoCrNiAl coating is more resistant to plastic deformations during the wear process, which in turn, translates into high wear resistance [33].

Table 3. Frictional wear performances of coatings with different Al contents.

Sample	COF	Worn Width/ μm	Worn Depth/ μm	Wear Rate/ $\text{mm}^3/(\text{Nm})$
Substrate	0.32	1674	168	6.79×10^{-8}
FeCoCrNi	0.62	1795	197	8.55×10^{-7}
FeCoCrNiAl _{0.5}	0.4	1732	186	6.53×10^{-7}
FeCoCrNiAl	0.1	1422	92	8.24×10^{-9}

Figure 8 displays the SEM images of worn surfaces and element distribution of the coatings after wear testings, and Figure 9 shows the reconstructed 3D morphologies of the worn surfaces of the substrates and the corresponding FeCoCrNiAl_x HEA coatings. The worn surface of FeCoCrNiAl looks the smoothest. SEM revealed large amounts of adhesion and debris on the worn surface of the FeCoCrNi coating (see Figure 8), corroborating the result above. Additionally, shallow grooves parallel to the sliding direction were also observed on the worn surface of the FeCoCrNi coating, which is typical for adhesive wear and abrasive wear patterns. Such patterns form because some metal pieces were removed from the softer parts of the coatings during the sliding of the ball against the coating. The adhesions form when a material is pushed by the ball and its residues move on the coating surface, leaving these parallel grooves [34]. When some adhesions remain stuck on the worn surface, and the rest are torn off, a “ridge”-fractured morphology forms [35]. Adhesions were rarely observed in Al-containing FeCoCrNiAl_x HEA coatings. However, the grooves were deeper. Small pits were also found in the FeCoCrNiAl HEA coating (see insert in Figure 8c), which confirms the abrasive nature of the wear process.

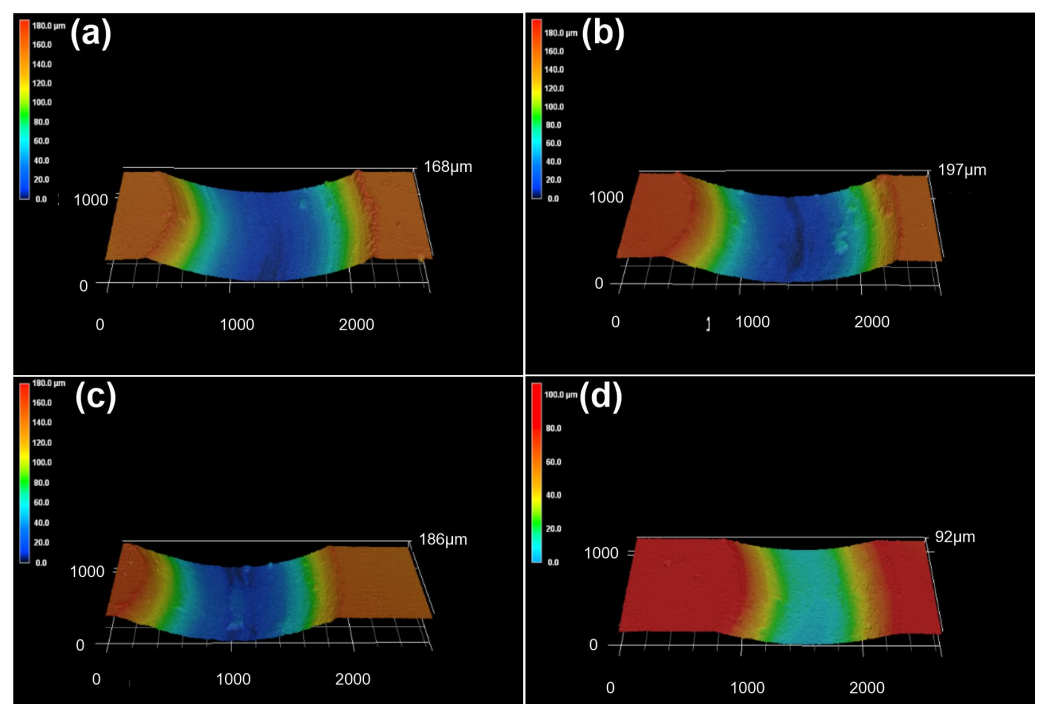


Figure 9. 3D morphologies of the worn surfaces of the (a) substrate, (b) FeCoCrNi, (c) FeCoCrNiAl_{0.5}, (d) FeCoCrNiAl.

EDS showed that O content in the debris was high at points A and B (see Figure 8d–f) very likely because of the formation of friction oxides due to the reaction between the debris and oxygen during the wear tests [36,37]. Thus, the wear mechanisms of FeCoCrNi and FeCoCrNiAl_{0.5} coatings also include oxidation wear. The strength of the FeCoCrNiAl coating was sufficiently high to resist plastic deformation. Thus, abrasive debris was rarely observed. However, fine pits were observed on the flat worn surface together with deep plow grooves, running parallel to the sliding direction. The worn surface of the FeCoCrNiAl coating contained the expected amount of oxygen according to the elemental EDS mapping of point C (Figure 8f). Thus, the wear mechanism of the FeCoCrNiAl coating included both abrasive and oxidative wear. These results again confirm that Al incorporation into the FeCoCrNi HEA coatings is very beneficial in improving its wear properties.

4. Conclusions

This work reports the laser cladding of FeCoCrNiAl_x HEA coatings with different Al contents. The microstructure and wear behaviors of these coatings were thoroughly characterized, and the following conclusions were achieved.

1. Laser cladding can fabricate high-quality FeCoCrNiAl_x HEA coatings with different Al contents. The dilution rate of cladding tracks increased from 22.5% to 33.1% as the Al content x increased from 0 to 1. The coatings exhibited minimum pores and excellent bonding to the substrate.
2. At Al content x in the FeCoCrNiAl_x HEA coating equal to one, the structure of initially FCC-structured FeCoCrNi and FeCoCrNiAl_{0.5} HEA coatings transitioned to single BCC-structure while the grain size decreased. The hardness for this coating (relative to Al-free one) increased from 202 to 546 HV_{0.2}, CoF decreased from 0.62 to 0.1, and wear rate decreased from 8.55×10^{-7} to 8.24×10^{-9} mm³/(Nm).
3. The wear mechanism of FeCoCrNi coating, determined by analyzing the wear surfaces by SEM, includes abrasive, adhesive, and oxidative wear. The wear mechanisms of the FeCoCrNiAl_{0.5} and FeCoCrNiAl coatings include only abrasive and oxidative wear. Thus, adding Al into FeCoCrNi significantly improves its wear properties.

Author Contributions: Y.L. Funding acquisition, Methodology, Writing—original draft. Z.X. Data curation, Investigation, Formal analysis, Writing—review and editing. G.X. Project administration, Resources, Writing—review and editing. H.C. Methodology, Writing—review and editing. All authors have read and agreed to the published version of the manuscript.

Funding: Major Projects of Scientific & Technological Innovation (2025) of Ningbo City (Grant No. 2019B10078). The authors also appreciate the supports from the Ningbo Institute of Zhongwu Laser and Photoelectric Technology.

Institutional Review Board Statement: Not applicable.

Informed Consent Statement: Not applicable.

Data Availability Statement: Not available.

Conflicts of Interest: The authors declare no conflict of interest.

References

1. Yeh, J.W.; Chen, S.K.; Lin, S.J.; Gan, J.Y.; Chin, T.S.; Shun, T.T.; Tsau, C.H.; Chang, S.Y. Nanostructured high-entropy alloys with multiple principal elements: Novel alloy design concepts and outcomes. *Adv. Eng. Mater.* **2004**, *6*, 299–303. [[CrossRef](#)]
2. Cantor, B.; Chang, I.T.H.; Knight, P.; Vincent, A.J.B. Microstructural development in equiatomic multicomponent alloys. *Mater. Sci. Eng. A* **2004**, *375*, 213–218. [[CrossRef](#)]
3. Xu, Y.; Li, W.; Qu, L.; Yang, X.; Song, B.; Lupoi, R.; Yin, S. Solid-state cold spraying of FeCoCrNiMn high-entropy alloy: An insight into microstructure evolution and oxidation behavior at 700–900 °C. *J. Mater. Sci. Technol.* **2021**, *68*, 172–183. [[CrossRef](#)]
4. Deng, Y.; Tasan, C.C.; Pradeep, K.G.; Springer, H.; Kostka, A.; Raabe, D. Design of a twinning-induced plasticity high entropy alloy. *Acta Mater.* **2015**, *94*, 124–133. [[CrossRef](#)]
5. Otto, F.; Dlouhy, A.; Somsen, C.; Bei, H.; Eggeler, G.; George, E.P. The influences of temperature and microstructure on the tensile properties of a CoCrFeMnNi high-entropy alloy. *Acta Mater.* **2013**, *61*, 5743–5755. [[CrossRef](#)]

6. Xu, Y.K.; Li, Z.Y.; Liu, J.R.; Chen, Y.N.; Zhang, F.Y.; Wu, L.; Hao, J.M.; Liu, L. Microstructure evolution and properties of laser cladding CoCrFeNiTiAl_x high-entropy alloy coatings. *Coatings* **2020**, *10*, 373. [[CrossRef](#)]
7. Sharma, A. High entropy alloy coatings and technology. *Coatings* **2021**, *11*, 372. [[CrossRef](#)]
8. Sharma, A.; Deshmukh, S.A.; Liaw, P.K.; Balasubramanian, G. Crystallization kinetics in Al_xCrCoFeNi (0 ≤ x ≤ 40) high-entropy alloys. *Scr. Mater.* **2017**, *141*, 54–57. [[CrossRef](#)]
9. Ogura, M.; Fukushima, T.; Zeller, R.; Dederichs, P.H. Structure of the high-entropy alloy Al_xCrFeCoNi: Fcc versus bcc. *J. Alloys Compd.* **2017**, *715*, 454–459. [[CrossRef](#)]
10. Feng, X.B.; Fu, W.; Zhang, J.Y.; Zhao, J.T.; Li, J.; Wu, K.; Liu, G.; Sun, J. Effects of nanotwins on the mechanical properties of Al_xCoCrFeNi high entropy alloy thin films. *Scr. Mater.* **2017**, *139*, 71–76. [[CrossRef](#)]
11. Hsu, C.Y.; Sheu, T.S.; Yeh, J.W.; Chen, S.K. Effect of iron content on wear behavior of AlCoCrFe_xMo_{0.5}Ni high-entropy alloys. *Wear* **2010**, *268*, 653–659. [[CrossRef](#)]
12. Jin, G.; Cai, Z.B.; Guan, Y.J. High temperature wear performance of laser-cladded FeNiCoAlCu high-entropy alloy coating. *Appl. Surf. Sci.* **2018**, *445*, 113–122. [[CrossRef](#)]
13. Zhu, Y.; Guo, X.Y.; Wen, C. Effect of annealing temperature on the thermal stability of FeCrNiMnMo_xSi_{0.5}B_{0.5} coatings. *Surf. Eng.* **2019**, *35*, 962–969. [[CrossRef](#)]
14. Cai, Y.C.; Zhu, L.S.; Cui, Y. Fracture and wear mechanisms of FeMnCrNiCo+xTiC composite high-entropy alloy cladding layers. *Appl. Surf. Sci.* **2020**, *543*, 148794. [[CrossRef](#)]
15. Li, X.F.; Feng, Y.H.; Liu, B. Influence of NbC particles on microstructure and mechanical properties of AlCoCrFeNi high-entropy alloy coatings prepared by laser cladding. *J. Alloys Compd.* **2019**, *788*, 485–494. [[CrossRef](#)]
16. Wu, T.; Chen, Y.X.; Lin, B.; Yu, L.T.; Gui, W.Y.; Li, J.H.; Wu, Y.; Zeng, D.W. Effects of WC on the microstructure, wear and corrosion resistance of laser-deposited CoCrFeNi high entropy alloy coatings. *Coatings* **2022**, *12*, 985. [[CrossRef](#)]
17. Hao, W.J.; Sun, R.L.; Niu, W.; Li, X.L.; Gu, M.; Zuo, R.Y. Study on microstructure and corrosion resistance of CoCrFeNiSi_x high-entropy alloy coating by laser cladding. *Surf. Technol.* **2020**, *50*, 343–348.
18. Bao, Y.Y.; Ji, X.L.; Gu, P.; Zhao, J.H. Effect of aluminum content on the microstructure and erosion wear resistance of FeCrNiCoCu high-entropy alloy coatings. *Tribology* **2017**, *37*, 421–428.
19. Liu, H.; Gao, Q.; Dai, J.B.; Chen, P.J.; Gao, W.P.; Hao, J.B.; Yang, H.F. Microstructure and high-temperature wear behavior of CoCrFeNiW_x high-entropy alloy coatings fabricated by laser cladding. *Tribol. Int.* **2022**, *172*, 107574. [[CrossRef](#)]
20. Liu, H.; Gao, Q.; Gao, W.P.; Liu, X.B.; Hao, J.B.; Yang, H.F. High temperature tribological properties of CoCrFeNiNb_x high-entropy alloy coatings by laser cladding. *Tribology* **2022**, *42*, 966–977.
21. Munitz, A.; Salhov, S.; Hayun, S. Heat treatment impacts the micro-structure and mechanical properties of AlCoCrFeNi high entropy alloy. *J. Alloys Compd.* **2016**, *683*, 221–230. [[CrossRef](#)]
22. Kumar, N.A.P.K.; Li, C.; Leonard, K.J.; Bei, H.; Zinkle, S.J. Microstructural stability and mechanical behavior of FeNiMnCr high entropy alloy under ion irradiation. *Acta Mater.* **2016**, *113*, 230–244. [[CrossRef](#)]
23. Lee, C.P.; Chang, C.C.; Chen, Y.Y.; Yeh, J.W.; Shih, H.C. Effect of the aluminium content of Al_xCrFe_{1.5}MnNi_{0.5} high-entropy alloys on the corrosion behaviour in aqueous environments. *Corros. Sci.* **2008**, *50*, 2053–2060. [[CrossRef](#)]
24. Guo, W.M.; Ding, N.; Liu, G.Q.; Jing, C.N.; Xu, H.X.; Liu, L.; Xu, N.; Wu, X.F.; He, J.Q.; Zairi, F. Microstructure evolution of a multi-track AlCoCrFeNi high entropy alloy coating fabricated by laser cladding. *Mater. Charact.* **2022**, *184*, 111660. [[CrossRef](#)]
25. Zhou, Y.J.; Zhang, Y.; Wang, Y.L.; Chen, G.L. Microstructure and compressive properties of multicomponent Al_x(TiVCrMnFeCoNiCu)_{100-x} high-entropy alloys. *Mater. Sci. Eng. A* **2007**, *454–455*, 260–265. [[CrossRef](#)]
26. Wang, W.R.; Wang, W.L.; Yeh, J.W. Phases, microstructure and mechanical properties of Al_xCoCrFeNi high-entropy alloys at elevated temperatures. *J. Alloys Compd.* **2014**, *589*, 143–152. [[CrossRef](#)]
27. Joseph, J.; Jarvis, T.; Wu, X.; Stanford, N.; Hodgson, P.; Fabijanic, D.M. Comparative study of the microstructures and mechanical properties of direct laser fabricated and arc-melted Al_xCoCrFeNi high entropy alloys. *Mater. Sci. Eng. A* **2015**, *633*, 184–193. [[CrossRef](#)]
28. Kühn, G.W.; Kurz, D.J. Fundamentals of Solidification. *Cryst. Res. Technol.* **1986**, *21*, 1176. [[CrossRef](#)]
29. Straumal, B.B.; Klinger, L.; Kuzmin, A.; Lopez, G.A.; Korneva, A.; Straumal, A.B.; Vershinin, N.; Gornakova, A.S. High entropy alloys coatings deposited by laser cladding: A review of grain boundary wetting phenomena. *Coatings* **2022**, *12*, 343. [[CrossRef](#)]
30. Cai, Y.C.; Zhu, L.S.; Cui, Y.; Geng, K.P.; Manladan, S.M.; Luo, Z. High-temperature oxidation behavior of FeCoCrNiAl_x high-entropy alloy coatings. *Mater. Res. Express* **2019**, *6*, 126552. [[CrossRef](#)]
31. Cai, Y.C.; Zhu, L.S.; Cui, Y.; Geng, K.P.; Han, T.F.; Manladan, S.M.; Luo, Z.; Han, J. Influence of high-temperature condition on the microstructure and properties of FeCoCrNiAl_{0.3} and FeCoCrNiAl_{0.7} high-entropy alloy coatings. *Surf. Eng.* **2021**, *37*, 179–187. [[CrossRef](#)]
32. Shi, Y.; Yang, B.; Xie, X.; Brechtel, J.; Dahmen, K.A.; Liaw, P.K. Corrosion of Al_xCoCrFeNi high entropy alloys: Al-content and potential scan-rate dependent pitting behavior. *Corros. Sci.* **2017**, *119*, 33–45. [[CrossRef](#)]
33. Schino, A.D.; Kenny, J.M. Effects of the grain size on the corrosion behavior of refined AISI 304 austenitic stainless steels. *J. Mater. Sci. Lett.* **2002**, *21*, 1631–1634. [[CrossRef](#)]
34. Yao, L.; He, Y.Q.; Wang, Z.Q.; Peng, B.Y.; Li, G.P.; Liu, Y. Effect of heat treatment on the wear properties of selective laser melted Ti-6Al-4V alloy under different loads. *Acta Metall. Sin.-Engl.* **2022**, *35*, 517–525. [[CrossRef](#)]

35. Tang, Y.M.; Zuo, Y.; Wang, J.N.; Zhao, X.H.; Niu, B.; Lin, B. The metastable pitting potential and its relation to the pitting potential for four materials in chloride solutions. *Corros. Sci.* **2014**, *80*, 111–119. [[CrossRef](#)]
36. Li, X.X.; Zhang, Q.Y.; Zhou, Y.; Liu, J.Q.; Chen, K.M.; Wang, S.Q. Mild and Severe Wear of Titanium Alloys. *Tribol. Lett.* **2016**, *61*, 14. [[CrossRef](#)]
37. Li, X.X.; Zhou, Y.; Ji, X.L.; Li, Y.X.; Wang, S.Q. Effects of sliding velocity on tribo-oxides and wear behavior of Ti-6Al-4V alloy. *Tribol. Int.* **2015**, *91*, 228. [[CrossRef](#)]

Disclaimer/Publisher's Note: The statements, opinions and data contained in all publications are solely those of the individual author(s) and contributor(s) and not of MDPI and/or the editor(s). MDPI and/or the editor(s) disclaim responsibility for any injury to people or property resulting from any ideas, methods, instructions or products referred to in the content.